

Cross-Domain Knowledge Distillation for Low-Resolution Human Pose Estimation

Zejun Gu, Zhong-Qiu Zhao, Henghui Ding, Hao Shen, Zhao Zhang, *Senior Member, IEEE*, and De-Shuang Huang, *Fellow, IEEE*

Abstract—In practical applications of human pose estimation, low-resolution inputs frequently occur, and existing state-of-the-art models perform poorly with low-resolution images. This work focuses on boosting the performance of low-resolution models by distilling knowledge from a high-resolution model. However, we face the challenge of feature size mismatch and class number mismatch when applying knowledge distillation to networks with different input resolutions. To address this issue, we propose a novel cross-domain knowledge distillation (CDKD) framework. In this framework, we construct a scale-adaptive projector ensemble (SAPE) module to spatially align feature maps between models of varying input resolutions. It adopts a projector ensemble to map low-resolution features into multiple common spaces and adaptively merges them based on multi-scale information to match high-resolution features. Additionally, we construct a cross-class alignment (CCA) module to solve the problem of the mismatch of class numbers. By combining an easy-to-hard training (ETHT) strategy, the CCA module further enhances the distillation performance. The effectiveness and efficiency of our approach are demonstrated by extensive experiments on two common benchmark datasets: MPII and COCO. The code is made available in supplementary material.

Index Terms—Knowledge distillation, low-resolution image, human pose estimation, cross-domain distillation.

I. INTRODUCTION

HUMAN pose estimation (HPE) is a fundamental task in computer vision which aims to predict the positions of body joints from RGB images [23], [31], [68]–[70], [90]. The recent progress has focused on training methods [29], [33], network structures [3], [8], [32], and fusion strategies [30], which have notably advanced the accuracy of HPE with high-resolution images [117]–[121].

In real-world application scenarios, images are usually captured in low resolutions, for example, wide-view video surveillance and long-distance shooting. In addition, high-resolution input will bring great computational and memory complexity, which impedes the development of practical applications. However, when current state-of-the-art models are directly applied to low-resolution images, significant performance degradation occurs due to the lack of rich image information. Therefore, it is a critical yet more challenging

Zejun Gu, Zhong-Qiu Zhao, Hao Shen, and Zhao Zhang are with the School of Computer Science and Information Engineering, Hefei University of Technology, Hefei 230009, China. (e-mail: guzejunmail@gmail.com, haoshenhs@gmail.com; cszzhang@gmail.com; Corresponding author: Zhong-Qiu Zhao)

Henghui Ding is with the School of Computer Science, Fudan University, Shanghai 200433, China (e-mail: henghui.ding@gmail.com)

De-Shuang Huang is with the Institute of Machine Learning and Systems Biology, Eastern Institute of Technology (e-mail: huangdeshuang@163.com)

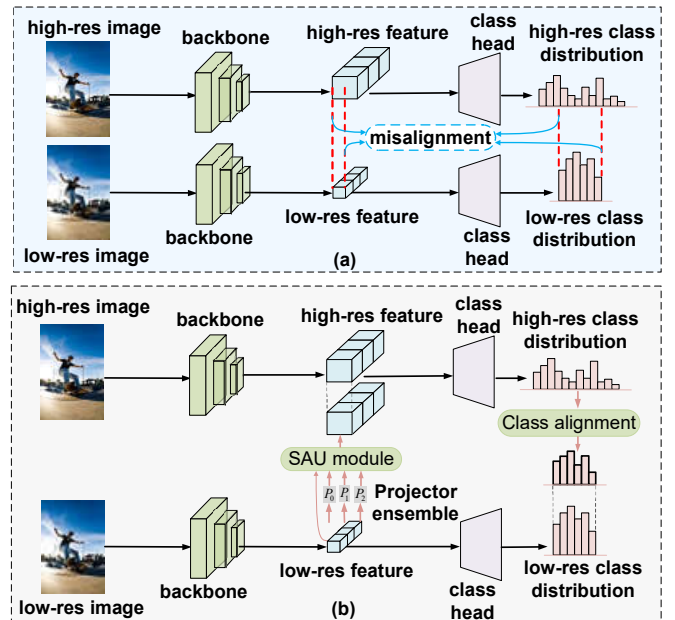


Fig. 1. Comparison between traditional distillation and our CDKD. (a) Illustration of the issue of traditional methods for distillation between different resolution models. When distilling knowledge from high-res models to low-res models, there is a problem of misalignment between features and output classes. (b) The overview of our proposed CDKD framework.

problem to upgrade the performance of a low-resolution HPE model. One possible way to solve the problem is to transfer the knowledge from high-res models to low-res models.

However, the different input resolutions of the teacher model and the student model lead to the following two problems: 1) The teacher model and the student model do not share the same feature spatial size at the same network stages. In this situation, traditional feature distillation methods can not work. 2) The number of output categories of the teacher model and the student model are not the same. Currently, there are *NO* logit distillation studies based on different class numbers in detection tasks, so the logit information in teacher models can not be effectively distilled.

Due to the mismatch in the feature spatial domain and output distribution domain between the teacher model and the student model, we propose a novel knowledge distillation framework termed cross-domain knowledge distillation (CDKD) to resolve it. It mainly includes the following two components: 1) A scale-adaptive projector ensemble (SAPE) module for feature distillation. 2) A cross-class alignment

(CCA) module for logit distillation.

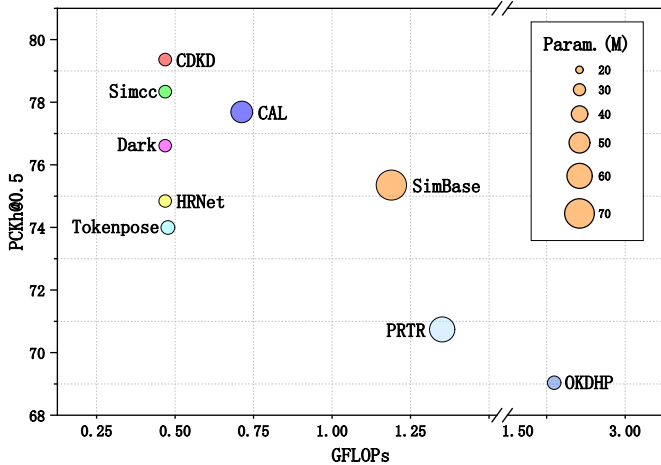


Fig. 2. Comparisons between the SOTA methods and the proposed CDKD on the MPII [2] val dataset with the input resolution of 64×64 . Red circles at the upper left corner denote CDKD. It outperforms SOTA models in terms of accuracy (AP), Parameter, and computational cost (GFLOPs).

The SAPE module resolves the feature size mismatch between the high-res teacher and the low-res student. Firstly, we design a projector to map features into a common space for matching. Feature distillation can be regarded as a multi-task learning process, including feature learning for the original task and feature matching for distillation [18]. In this scenario, the student network might overfit the teacher’s feature distributions, leading to less distinguishable generated features for HPE. Adding a projector for distillation would alleviate the overfitting issue. We propose to ensemble projectors for further improvement. According to the theory about ensemble learning [12], different initialized projectors produce different transformed features. The use of multiple projectors helps to improve the generalization ability of the student. To address the body scale variation problem in the natural scene, we propose a scale-adaptive unit (SAU) to capture the multi-scale information. It assigns different weights to each projector by multiple parallel transformations with different receptive fields. Then, it merges the output features of each projector with assigned weights.

The CCA module solves the problem of class number mismatch. As shown in Fig. 1 (b), the probability distribution of the classification output for different resolution models has the same mathematical significance. It can be shared directly between the teacher model and the student model. Meanwhile, the probability values of multiple adjacent classes can be merged by adding them together. In addition, the probability distribution of the classification output is also a fundamental element in calculating distillation loss. Based on this observation, for the high-res teacher, we merge the probability values of adjacent categories to make them consistent with the categories of the student model. It allows for the implementation of logit distillation. Finally, to enhance the effectiveness of distillation, we further propose an easy-to-hard training (ETHT) strategy. It improves distillation performance through curriculum learning.

In summary, our CDKD achieves optimal performance with minimal computational cost. As shown in Fig. 2, CDKD outperforms previous SOTA methods, such as Simcc [10] and CAL [6] with few parameters and GFLOPs.

Our contributions are summarized as follows:

- We propose a novel scale-adaptive projector ensemble (SAPE) module that solves the problem of feature size mismatch between the high-res teacher and the low-res student and attains excellent distillation performance.
- We construct a cross-class alignment (CCA) module to tackle the problem of inconsistent class numbers in logit distillation. Combined with the easy-to-hard training (ETHT) strategy, it further improves the distillation effectiveness.
- Our proposed CDKD is a universal framework that can address the issue of mismatched feature spatial domain and output distribution domain in different distillation tasks. Extensive experiment results demonstrate its efficiency, effectiveness, and universality. It achieves SOTA performance in low-res HPE on MPII [2] and COCO [1] with *NO* computational cost increment. When applied to different HPE models and various low-res inputs, it consistently achieves superior performance.

II. RELATED WORK

A. Human Pose Estimation

The current research on human pose estimation primarily focuses on two aspects: keypoint coordinate representation and applications under complex conditions.

For keypoint coordinate representation, recent works are mainly divided into three mainstreams: regression-based methods [9], [11], [56]–[59], heatmap-based methods [4], [5], [8], [52], [53], [75], [76], and new keypoint representation methods [10], [23]. Regression-based methods directly regress the coordinates of keypoints within a lightweight framework. Deeppose [59] is the first to propose direct regression of joint coordinates. CenterNet [60] presents a method to accomplish multi-person pose estimation within a one-stage object detection framework, directly regressing joint coordinates instead of bounding boxes. SPM [107] introduces root joints for distinguishing among different person instances, by employing hierarchical rooted representations of human body joints to improve the prediction of long-range displacements for specific joints. The residual log-likelihood (RLE) [11] utilizes normalizing flows to capture the underlying output distribution, which enables regression-based methods to achieve accuracy comparable to SOTA heatmap-based methods. MDN [77] proposes a mixture density network for regression. Regression-based methods have significant advantages in speed, but their accuracy is insufficient.

The heatmap-based methods adopt a two-dimensional Gaussian distribution to represent joint coordinates. Some studies optimize backbones to extract better features. Sun *et al.* [3] introduce a groundbreaking network designed to preserve high-resolution representations throughout the entirety of the process, resulting in substantial performance enhancements.

Other studies aim to improve prediction accuracy by reducing quantization errors. Zhang *et al.* [6] propose using a distribution-aware coordinate representation for post-processing of prediction results to reduce quantization errors. Huang *et al.* [49] design a plug-and-play unbiased data processing method that effectively enhances the performance of different models without increasing computational complexity. Some methods [8], [69] improve their performance by leveraging transformers because they can capture long-range information. Heatmap-based methods are far ahead in terms of performance, but they have the disadvantage of exceptionally high computational cost and slow preprocessing operations. DistilPose [31] combines heatmap and regression methods through knowledge distillation, achieving high accuracy at low computational costs.

New keypoint representation methods explore novel approaches of keypoint representation to reduce quantization errors and leverage keypoint relationships. PCT [23] represents a pose by discrete tokens to model the dependency between the body joints. Simcc [10] effectively minimizes quantization error by transforming the keypoint regression task into a classification problem. They all open up new perspectives on keypoint representation methods.

In addition, many studies are beginning to focus on applications under complex conditions. Yang *et al.* [99] introduce ED-Pose, which achieves fast, concise, and accurate end-to-end human pose estimation. Lee *et al.* [97] present ExLPose to tackle the problem of current models failing to work properly under low-light conditions. Ju *et al.* [98] propose a dataset for human pose estimation in artwork, aiming to apply the human pose estimation model to virtual scenes. Yang *et al.* [25] introduce an efficient full-body pose estimation method (DWPose), aiming at better application in human-computer interaction. Sun *et al.* [108] propose the first all-in-one-stage model for expressive human pose and shape estimation, which achieves the best performance.

B. Low-Resolution Vision Tasks

Wang *et al.* [6] propose a novel confidence-aware learning (CAL) method to reduce quantization errors, thereby improving the performance of human pose estimation models under low-resolution conditions. Li *et al.* [10] design a simple coordinate classification method, which achieves excellent results in low-resolution pose estimation by transforming coordinate regression into a classification problem. Kumar *et al.* [38] present a semi-supervised approach to predict landmarks on low-resolution images by learning them from labeled high-resolution images. It can improve performance on the critical task of face verification in low-resolution images. Chai *et al.* [39] introduce a recognizability embedding enhancement approach to address the very low-resolution face recognition (VLRFR) challenge. Sunkara *et al.* [40] design a new CNN building block (SPD) for low-resolution images and small objects. This block is universal and can replace the downsampling layers in different CNN models, thereby improving the performance of various low-resolution tasks. Xu *et al.* [41] propose a resolution-aware neural network for human pose

estimation which can deal with different resolution images with a single model.

C. Knowledge Distillation

Knowledge distillation aims to transfer knowledge from a trained teacher model to a compact and lightweight student model. In recent years, various methods have been proposed for knowledge distillation [24], [25], [35]. These methods fall into two lines of work: 1) feature distillation methods [26]. 2) logit distillation methods [27]. Feature distillation methods distill knowledge using intermediate features, while logit distillation methods are designed to perform distillation on output logits.

Logit distillation was originally proposed using the KL divergence [109], and it has been extended using spherical normalization [115], label decoupling [27], and probability reweighting [116]. MLD [16] introduces a multi-level prediction alignment framework to logit distillation. Through this framework, the student model learns instance prediction, input correlation, and category correlation simultaneously. LD [44] presents a novel localization distillation (LD) method that can efficiently transfer the localization knowledge from the teacher to the student.

While logit distillation methods may seem straightforward and versatile for application across various scenarios, their performance frequently falls short compared to feature distillation. Compared to logit distillation, feature distillation methods are more likely to achieve high performance because they absorb rich knowledge from the teacher model. The work [42] adopts a novel orthogonal projection layer to maximize the distilled knowledge to the student backbone, thereby achieving outstanding performance. CrossKD [43] transfers the intermediate features from the student's head to that of the teacher, generating crosshead predictions for distillation. This approach efficiently mitigates conflicts between supervised and distillation targets. Some methods [110], [111] mitigate the differences in features between the teacher and student models, thus compelling the student model to emulate the teacher model at the feature level. Other methods [112], [113] transmit teacher knowledge by extracting input correlations.

In contrast to existing KD methods that focus on improving the performance of lightweight networks, this paper aims to improve the low-res model by distilling from the high-res model. Recently, a succession of relevant studies has emerged. The work [13] adopts a multi-scale aligned distillation method to tackle the output size mismatch, but this method relies on the feature pyramid (FPN) structure [114] as its backbone. The distillation method improves the low-res model by using upsampling in the initial stage [15]. However, upsampling introduces noise and incurs substantial computational costs. FMD [14] solves the problem of inconsistent feature sizes, but it is under the limited condition that the number of channels will not remain constant. FITNETS [36] utilizes convolutional downsampling to align high-res features with their low-res counterparts. Nonetheless, downsampling drastically reduces the rich efficient information hidden in large feature maps. ScaleKD [24] designs a mapping function to align the size of

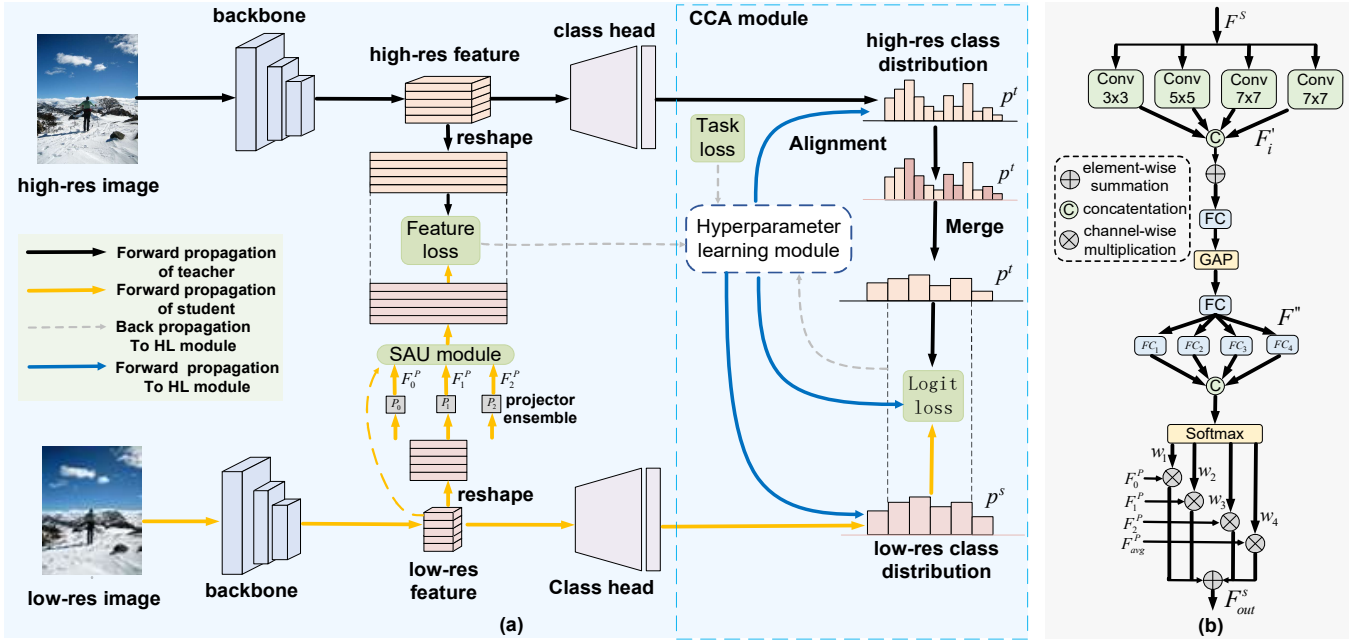


Fig. 3. (a) Overall architecture of our proposed CDRD. During training, a well-trained and fixed high-res teacher provides rich knowledge to help the training of a low-res student based on the alignment of features and classes. (b) The illustration of our SAU module.

the feature map in different models, but it does not achieve outstanding performance. Our proposed method (CDKD) can solve the above problems and thereby achieve more competitive distillation effects.

III. METHOD

In this section, we propose a distillation-based human pose estimation framework, cross-domain knowledge distillation (CDKD), as shown in Fig. 3 (a). In CDKD, the teacher is a high-res model, and the student is a low-res model. We transfer the rich details and texture knowledge from the teacher model to the student model during training.

A. Scale-Adaptive Projector Ensemble

The Scale-Adaptive Projector Ensemble (SAPE) aims to align the feature size of the teacher and the student, which consists of a projector ensemble and a scale-adaptive unit.

1) *Projector Ensemble* : As shown in Fig. 3 (a), our framework is based on the Simcc [10] algorithm. Recent research indicates that feature distillation is more likely to achieve superior performance compared to logit distillation [16]. The last feature of networks is better suited for distillation [17]. One possible reason is that the last feature is closer to the classifier and will directly impact classification effectiveness. Therefore, we adopt the last feature to distill.

We represent the last teacher feature as $F^t \in \mathbb{R}^{B \times C \times H' \times W'}$, where B , C , H' , and W' are the batch size, the number of channels, the height, and the width of the last teacher feature maps, respectively. The corresponding student feature is represented by $F^s \in \mathbb{R}^{B \times C \times H \times W}$, where B , C , H , and W are the batch size, the number of channels, the height, and the width of the last student feature maps, respectively.

We define m as the scale factor between the high and low resolution, where $H = H'/m$ and $W = W'/m$.

In classification tasks based on distillation, the training process of the student network can be considered as multi-task learning within the same feature space. Therefore, student features are prone to overfit teacher features and would be less discriminative for classification. We add a projector P_i to disentangle the two tasks to improve the student's performance and to match the size of F^t (see Fig. 3 (a)). In addition, we use an ensemble of projectors for further improvement which consists of a group of parallel projectors. Each projector contains a FC layer and a ReLU function.

There are two motivations for adopting ensemble projectors. 1) Projectors with diverse initializations yield distinct transformed features, contributing to the generalizability of the student. 2) The projected student features may include zeros due to the use of the ReLU function in the projector. In contrast, teacher features are less likely to be zeros since the average pooling operation is widely employed in CNNs. The feature distribution gap between the teacher model and the student model is large when using a single projector. In this paper, we use ensemble learning to reduce the feature distribution gap and achieve better generalizability.

2) *Scale-Adaptive Unit* : The previous work [18] uses a simple additive approach to fuse output features from different projectors. The simple additive approach not only fails to capture multi-scale information in real-world scenarios but also lacks the weight assignment based on the importance of different projectors. Inspired by [20], we propose the scale-adaptive unit (SAU) to deal with the problem. The SAU learns to combine all outputs from different projectors to produce a rich output feature. It is composed of multiple parallel transformations with different receptive fields, exploiting local

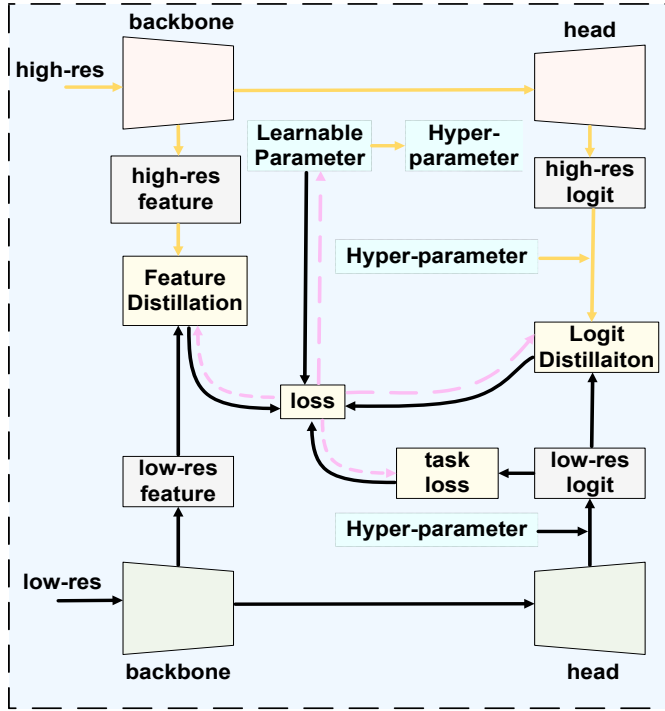


Fig. 4. The illustration of our proposed easy-to-hard training (ETHT) strategy.

and global information to obtain a strong low-res feature.

The architecture of the proposed SAU is depicted in Fig. 3 (b). We take the output of each projector and the low-res feature as input of SAU. Initially, we operate it through convolutions with different kernel sizes:

$$F'_i = Conv_i(F^s) \quad (1)$$

where $Conv_i(\cdot)$ denotes convolution operation with different kernel sizes, F^s is the last student feature, F'_i is output of each convolution operation and i is the index of each branch.

Convolutions with different receptive fields help the model to obtain human body information at different scales. Because low-res images contain less useful information, the feature information under a small receptive field does not make sufficient sense. Therefore, we moderately increase the proportion of convolutions with a large receptive field to obtain as much useful information as possible, as shown in Table VIII. Next, we fed F'_i to fusion operation:

$$F'' = Fus(Concat[F'_1, F'_2, F'_3, F'_4]) \quad (2)$$

where $Concat[\cdot]$ and $Fus(\cdot)$ denote the concatenation operation and the fusion operation, respectively. This fusion operation is sequentially composed of a fully connected layer, a global pooling layer, and a summation layer. It can adaptively adjust receptive field sizes according to the image content. Then, F'' is applied to select operation:

$$w_k = Select(F'') \quad (3)$$

where $Select(\cdot)$ is the select operation and w_k is the weight value corresponding to each projector output. The select operation is sequentially composed of multiple fully connected

layers, a concatenation layer, and a softmax layer. This operation can adaptively select different spatial scales of information with soft attention across channels. Finally, we fuse outputs from multiple projectors via an element-wise summation to obtain the output feature F_{out}^s :

$$F_{out}^s = \sum_{k=1}^K w_k \otimes F_k^P \quad (4)$$

where K is the number of branches, F_k^P is the output of each projector, w_k is the corresponding weight value, and F_{out}^s is the final output of this module.

After aligning features from multi-scale spaces, we can use cosine distance between F_{out}^s and F^t to calculate the feature distillation loss :

$$L_{fea} = 1 - \frac{F_{out}^s}{\|F_{out}^s\|_2} \cdot \frac{F^t}{\|F^t\|_2} \quad (5)$$

where $\|\cdot\|_2$ denotes L2-norm.

B. Cross-Class Alignment

Another way to transfer knowledge from teacher to student is logit distillation. The feature distillation focuses on optimizing the encoder and does not directly impact the classification head, so we propose a cross-class alignment (CCA) module to refine the student's classification head straightforwardly.

1) *Class Alignment* : As is shown in Fig. 1 (a), the number of Simcc's output categories is proportional to the input resolution typically. The number of output categories of low-res model and high-res model is different when their resolution is different. However, the current logit distillation is based on the consistency of the number of categories. In our work, we propose a cross-class (CCA) alignment module to resolve this issue.

Simcc's classification method can be regarded as one of ordinal regression [19]. There is a certain ordinal relationship among the categories in ordinal regression. Any number of adjacent classes can form an entire meaningful interval. We are interested in exploring the merging of multiple discrete categories of the student to align with the teacher. However, the values of the logit or the feature can not be added together, since they do not have the same computational unit and interpretable real-world meaning.

Combining the characteristics of ordinal regression and the properties of probability distributions, we have the following findings: 1) After the last softmax function, the values of the probability distribution can be added together. 2) The final output distribution of the model represents the probability of the keypoint at each relative position. Regardless of the resolution of images or the number of categories output by the model, the relative positions of keypoints in images are the same. 3) The output probability distributions of images at different resolutions have the same units and practical significance. So they can be shared between different resolution models. 4) The probability distribution output by the model is also the subject of computation for traditional logit distillation loss which serves as the bridge connecting the teacher model and

TABLE I
COMPARISON WITH SOTA METHODS ON THE MPII VAL DATASET.

Method	Input Size	Backbone	Head↑	Sho.↑	Elb↑	Wri.↑	Hip↑	Knee↑	Ank.↑	PCKh@0.5↑	Params (M)↓	FLOPs (G) ↓
SimBase [4]		ResNet-152	40.894	48.217	33.953	21.742	44.608	31.353	22.650	36.786	68.6	0.328
SimBase [4]		ResNet-50	41.473	49.474	34.839	22.393	45.837	32.541	23.405	37.780	34.0	0.187
HRNet [3]		HRNet-W32	46.044	52.378	40.191	28.407	48.780	37.176	27.538	42.217	28.5	0.148
Dark [5]		HRNet-W32	38.984	61.804	46.191	31.867	61.277	45.234	28.839	48.137	28.5	0.148
CAL [6]	32x32	HRNet-W32	77.115	68.631	48.185	33.066	63.164	46.264	40.552	55.353	49.3	0.209
Tokenpose [8]		HRNet-W32	38.950	61.702	47.537	31.902	61.676	45.476	28.600	48.421	30.9	0.152
PRTR [9]		HRNet-W32	0.341	1.512	8.062	9.082	15.977	1.633	0.213	5.618	57.2	1.476
Simcc (baseline) [10]		HRNet-W32	81.105	72.690	54.219	37.898	63.822	51.380	46.552	59.560	28.5	0.148
CDKD (ours)		HRNet-W32	83.049	74.711	56.213	41.427	64.999	52.589	48.724	61.442 _{+1.882}	28.5	0.148
SimBase [4]		ResNet-152	89.905	85.258	73.854	64.058	76.216	68.628	62.659	75.353	68.6	1.314
OKDHP [7]		4-Stack HG	85.573	80.757	66.099	54.328	71.767	61.032	54.393	69.037	30.9	2.899
HRNet [3]		HRNet-W32	90.075	85.785	72.950	63.511	75.143	67.257	61.880	74.843	28.5	0.593
Dark [5]		HRNet-W32	89.802	87.568	75.251	64.112	78.726	69.616	63.628	76.612	28.5	0.593
CAL [6]	64x64	HRNet-W32	92.497	88.689	75.763	65.019	80.076	70.159	65.422	77.692	49.3	0.837
Tokenpose [8]		HRNet-W32	89.018	86.770	71.570	59.963	77.237	65.947	59.139	73.997	31.0	0.602
PRTR [9]		HRNet-W32	89.768	83.967	68.144	53.061	76.112	62.039	53.660	70.742	57.2	1.476
Simcc (baseline) [10]		HRNet-W32	93.111	88.808	77.280	67.604	79.072	70.400	66.107	78.340	28.6	0.593
CDKD (ours)		HRNet-W32	93.622	89.844	78.422	68.137	80.820	71.991	66.438	79.362 _{+1.022}	28.6	0.593

the student model. Therefore, we adopt the class alignment method to align the category of different resolution models, as shown in Fig. 3 (a). Specially, we sum up the output probability values for every m adjacent categories in the high-res teacher model:

$$\mathbf{p}_j^t = \sum_{i=j \times m + 1}^{j \times m + m} \mathbf{p}_i^t \quad (6)$$

where m represents the ratio between high resolution and low resolution, \mathbf{p}_i^t denotes the output probability values of i -th category in the high-res model, \mathbf{p}_j^t is the j -th probability values after mergers. Then, the teacher model and the student model achieves class alignment, and logit distillation can be performed between them. Based on the above results, we can calculate the logit distillation loss:

$$L_{logit}(\mathbf{p}^t, \mathbf{p}^s, \tau) = \sum_{j=1}^J \tau^2 KL(\mathbf{p}_j^t, \mathbf{p}_j^s) \quad (7)$$

where τ is the temperature, \mathbf{p}^t and \mathbf{p}^s denote the output probability distribution produced by teacher and student, $KL(\cdot)$ is the Kullback-Leibler Divergence. With feature distillation loss L_{fea} and logit distillation loss L_{logit} , we can train the student with the total loss as:

$$L_{total} = L_{ori} + \alpha L_{fea} + \beta L_{logit} \quad (8)$$

where L_{ori} is the original task loss for HPE, α and β are the hyperparameters to balance the loss.

2) *Easy-to-Hard Training Strategy*: In human education, teachers often employ a curriculum strategy of imparting knowledge from simple to challenging, ensuring that students achieve optimal learning outcomes. Influenced by this, many researchers adopt the classic curriculum strategy training the models in an easy-to-hard method, which improves the performance of the models.

Inspired by CTKD [21], we adopt an easy-to-hard training (ETH) strategy to increase the difficulty gradually. As shown in Fig. 4, this strategy is implemented by adding a hyperparameter learning module to the student model. In this work, We choose temperature τ as the hyperparameter to be trained, which can also be extended to other hyperparameters, such as loss coefficient α and β (see Table VIII).

Firstly, this module is optimized in the opposite direction of the student’s training, intending to maximize the distillation loss between the student and teacher. It can enhance the training performance of the model by producing adversarial effects. We apply the gradient reversal method to implement the adversarial process. The traditional gradient descent process is as follows:

$$\theta \leftarrow \theta - \eta \frac{\partial L}{\partial \theta} \quad (9)$$

where θ is the training parameters, η is the learning rate, and L is the loss. Our proposed gradient reversal method is as follows:

$$\theta_{hype} \leftarrow \theta_{hype} + \eta \frac{\partial L}{\partial \theta_{hype}} \quad (10)$$

where θ_{hype} is the training hyperparameters. We optimize the hyperparameter module in the opposite direction of gradient descent, which essentially prevents loss from declining and increases the difficulty of model training. In addition, to gradually increase the training difficulty, we introduce a dynamic coefficient ξ in the above process of backpropagation.

$$\theta_{hype} \leftarrow \theta_{hype} + \eta \frac{\partial(\xi L)}{\partial \theta_{hype}} \quad (11)$$

$$\xi = func\left(\frac{T_i}{T_{max}}\right) \quad (12)$$

where $func(\cdot)$ denotes the monotonically increasing function, T_i is current epoch, and T_{max} is total epochs. As training

TABLE II
COMPARISON WITH SOTA METHODS ON THE COCO VALIDATION DATASET. (*) DENOTES THE EXPERIMENTAL RESULTS OBTAINED BY INCREMENTING THE SPLITTING FACTOR’S VALUE FOLLOWED BY SIMCC [10].

Method	Input size	Backbone	AP \uparrow	AP50 \uparrow	AP75 \uparrow	AP(M) \uparrow	AP(L) \uparrow	AR \uparrow	Params (M) \downarrow	FLOPs (G) \downarrow
HRNet [3]		HRNet-W32	8.2	36.9	1.3	9.2	6.8	15.0	28.5	0.148
TokenPose [8]		HRNet-W32	14.0	48.2	3.4	15.2	12.5	21.7	33.1	0.156
CAL [6]		HRNet-W32	26.4	61.9	18.2	27.1	25.7	33.9	49.3	0.209
Rle [11]		HRNet-W32	24.4	-	-	-	-	-	29.1	0.593
Dark [5]		HRNet-W32	12.5	45.2	2.5	13.8	11.1	20.3	28.5	0.148
SimBaese [4]	32x32	ResNet-152	4.4	21.1	1.0	5.3	3.2	9.0	68.6	0.328
PCT [23]		Swin-Base	1.3	4.6	10.0	1.0	1.2	3.1	86.9	1.676
Distillpose [31]		HRNet-W32	9.5	32.6	2.4	10.0	9.5	21.2	33.0	0.310
SimCC (<i>baseline</i>) [10]		HRNet-W32	29.8	65.6	22.5	30.0	29.9	36.3	28.5	0.148
CDKD (<i>ours</i>)		HRNet-W32	30.7 ^{+0.9}	66.4	23.5	30.9	30.7	37.3	28.5	0.148
SimpleBaseline [4]		ResNet-152	30.3	67.6	22.6	30.6	30.5	36.2	68.6	1.314
Distillpose [31]		HRNet-W32	31.7	66.8	26.6	32.3	31.8	44.5	33.1	0.790
PCT [23]		Swin-Base	13.8	41.1	6.4	14.1	14.2	19.6	86.9	2.300
Rle [11]		HRNet-W32	52.5	-	-	-	-	-	29.1	0.593
HRNet [3]	64x64	HRNet-W48	46.9	83.7	49.2	46.6	47.5	52.6	63.6	1.218
Tokenpose [8]		HRNet-W48	50.3	82.7	54.4	49.9	51.4	55.6	68.2	1.236
CAL [6]		HRNet-W48	60.6	88.1	68.4	59.5	62.3	65.5	110.3	1.797
Dark [5]		HRNet-W48	57.2	86.8	63.5	55.9	59.2	62.2	63.6	1.218
Simcc (<i>baseline</i>) [10]		HRNet-W48	58.6	85.9	64.9	57.8	60.5	63.4	63.7	1.218
CDKD (<i>ours</i>)		HRNet-W48	60.3 ^{+1.7}	86.9	67.3	59.6	62.0	65.0	63.7	1.218
Simcc (<i>baseline</i>)* [10]		HRNet-W48	59.7	85.0	67.3	58.4	64.0	67.5	63.7	1.218
CDKD (<i>ours</i>)*		HRNet-W48	61.1 ^{+1.4}	86.9	68.4	59.9	62.9	65.6	63.7	1.218

TABLE III

ABLATION STUDIES FOR DIFFERENT MODULES ON MPII VALIDATION SET. THE “NECM” MEANS THE NON-ETHHT CCA MODULE. ALL EXPERIMENTS USE HRNET-W32 AS THE BACKBONE AND TAKE IMAGES WITH 64 \times 64 RESOLUTION AS INPUT.

Method	SAPE		CCA			PCKh@0.5 \uparrow
	Projector	Ensemble	SAU	NECM	ETHHT	
Simcc (<i>baseline</i>) [10]	-	-	-	-	-	78.340
ours	✓					78.621
ours	✓	✓				78.717
ours	✓	✓	✓			78.808
ours				✓		78.772
ours				✓	✓	78.811
ours	✓	✓	✓	✓	✓	79.362

progresses, ξ gradually increases, and the training difficulty gradually increases. Therefore, by adopting this approach, the training performance is effectively optimized.

IV. EXPERIMENTS

In this section, we first evaluate the proposed distillation framework on two common benchmark datasets: MPII [2] and COCO [1]. Then we carry out a series of ablation studies to prove the effectiveness and validity of our approach. In addition, we show the universality of our proposed framework in various human pose estimation models.

A. Implementation Details

1) *Datasets*: The MPII dataset includes approximately 25K images containing over 40K subjects with annotated body joints, where 29K subjects are used for training and 11K subjects are used for testing. We adopt the same train/valid/test split as in [22]. Each person instance in MPII has 16 labeled joints. The PCKh@0.5 is used for the MPII dataset, which refers to a threshold of 50% of the head diameter.

The COCO dataset contains over 200k images and 250k human instances. Each human instance is labeled with $K = 17$ keypoints representing a human pose. Our models are trained on COCO train2017 with 57k images and evaluated on COCO val2017, which contain 5k and 20k images, respectively. We mainly report the commonly used standard evaluation metrics Average Precision (AP) and Average Recall (AR), which are calculated based on Object Keypoint Similarity (OKS) on the COCO dataset.

2) *Training Details*: We adopt the two-stage top-down human pose estimation pipeline. Firstly, the person instances are detected, and then the keypoints are estimated. In the stage of keypoint estimation, we set the cropped human images to low resolution. *We replicate SOTA human pose estimation methods under low-resolution conditions, following the settings detailed in their respective papers and code. When reproducing these SOTA researches, we only modify the resolution-related settings, leaving the others unchanged.* For all methods, we train and test under the same low resolution. We adopt a commonly used person detector provided by SimpleBaselines [4] with 56.4% AP for the MSCOCO val dataset. We utilize Simcc [10] as the base model for the teacher

and the student, which uses HRNet [3] as its backbone. In the case of SimpleBaseline [4], the base learning rate is initialized as $1e-3$. It is then decreased to $1e-4$ and $1e-5$ at the 90-th and 120-th epochs respectively.

TABLE IV

ABLATION STUDIES FOR DIFFERENT MODULES ON COCO VAL SET. THE “NECM” MEANS THE NON-ETHT CCA MODULE. ALL EXPERIMENTS USE HRNET-W32 AS THE BACKBONE AND TAKE IMAGES WITH 32×32 RESOLUTION AS INPUT.

Method	SAPE		CCA		AP \uparrow
	Projector	Ensemble	SAU	NECM ETHT	
Simcc (<i>baseline</i>) [10]	-	-	-	-	29.8
ours	✓				30.3
ours	✓	✓			30.4
ours	✓	✓	✓		30.6
ours				✓	30.3
ours				✓	30.6
ours	✓	✓	✓	✓	30.7

TABLE V

ABLATION STUDIES OF THE ALIGNMENT METHOD ON THE MPII VALIDATION DATASET. “CONV DOWNSAMPLE” AND “FULLY CONNECTED LAYER” MEAN CONVENTIONAL FEATURE AND CLASS ALIGNMENT METHODS, RESPECTIVELY. “SAME CLASS NUMBER” REFERS TO THE METHOD OF MAKING THE NUMBER OF CATEGORIES CONSISTENT BETWEEN THE TEACHER MODEL AND THE STUDENT MODEL BY ALTERING THE SPLITTING FACTOR [10].

Distillation	Method	PCKh@0.5 \uparrow
Feature distillation	Conv Downsample [36]	78.207
	Fully Connected Layer [24]	78.249
	Projector Ensemble (<i>ours</i>)	78.717
	SAPE (<i>ours</i>)	78.808
Logit distillation	Same Class Number [10]	75.173
	Fully Connected Layer [37]	77.973
	NECM (<i>ours</i>)	78.772
	CCA (<i>ours</i>)	78.811

As for HRNet [3], the base learning rate is also initialized as $1e-3$. It is subsequently reduced to $1e-4$ and $1e-5$ at the 170-th and 200-th epochs respectively. The total training processes conclude at the 140th and 210th epochs respectively for SimpleBaseline [4] and HRNet [3]. The training settings for CDKD, such as the optimizer, learning rate, and data augmentation, are the same as Simcc [10]. Experiments are conducted on 2 NVIDIA 3080-Ti GPUs.

B. Main Results

1) *Results on MPII Dataset:* We evaluate the CDKD framework on the MPII validation dataset. Table I compares the PCKh@0.5 accuracy results of CDKD and the SOTA methods under low-res conditions. We can clearly observe that Simcc [10] achieves outstanding performance with low computational cost. Adding CDKD, Simcc [10] is further improved. It achieves better accuracy than any other method. Specifically, in resolutions of 64×64 and 32×32 , our method

TABLE VI

ABLATION STUDIES OF THE PROJECTOR NUMBER ON THE MPII VALIDATION DATASET. THE PROJECTOR NUMBER REFERS TO THE NUMBER OF PROJECTORS IN THE SAPE MODULE.

Projector number	1	2	3	4	5
PCKh@0.5 \uparrow	78.621	79.037	79.362	76.937	76.831

TABLE VII

ABLATION STUDIES OF THE NUMBER OF CONVOLUTIONS WITH DIFFERENT KERNEL SIZES IN SAU ON THE MPII VALIDATION DATASET. THE 3×3 , 5×5 , 7×7 , AND 9×9 REFER TO THE CONV KERNEL SIZES.

Conv	3×3	5×5	7×7	9×9	PCKh@0.5 \uparrow
	1	1	1	0	78.972
Conv number	2	1	1	0	78.884
	3	1	1	0	78.519
	1	2	1	0	79.173
Conv number	1	1	2	0	79.362
	1	1	1	1	79.027

improves the baseline network by 1.022% and 1.882%, respectively.

It does not incur any additional costs in parameters and GFLOPs, The performance is significant as compared to prior works. In short, CDKD achieves SOTA performance with *NO* increase in computational cost.

2) *Results on COCO Dataset:* Table II shows the results of the cutting-edge methods and CDKD under low-res conditions on the COCO val2017 set. In resolutions of 32×32 and 64×64 , our method improves the baseline model 0.9% and 1.7%, respectively. Especially, it achieves SOTA performance, whether in a resolution of 32×32 or 64×64 . Meanwhile, it doesn’t bring any increase in computation and parameters. Our proposed CDKD method is an efficient and effective approach in low-res HPE.

C. Ablation Study

Different modules. In this subsection, we conduct several ablation experiments to show how each module helps the training of the low-res student. As shown in Table III, all modules benefit the low-res model. SAPE and CCA bring an improvement of 0.468% and 0.471%, respectively. In SAPE, the scale-adaptive unit (SAU) further improves the performance of the projector ensemble by 0.091%. Meanwhile, the CCA module brings the student 0.432% gains. When combing the ETHT strategy, the gains get to 0.471%. The combination of all proposed modules bring the best performance, which significantly improves the performance by 1.022%.

In order to thoroughly demonstrate the performance of the various modules proposed by us, we also conduct ablation experiments on the COCO dataset. As shown in Table IV, each module improves the model’s performance. The combination of all modules achieves the optimal performance for the model.

Alignment methods. We compare the results of CDKD with conventional feature alignment and class alignment in Table V. Projector ensemble and NECM both surpass conventional methods. On this basis, SAPE and CCA further

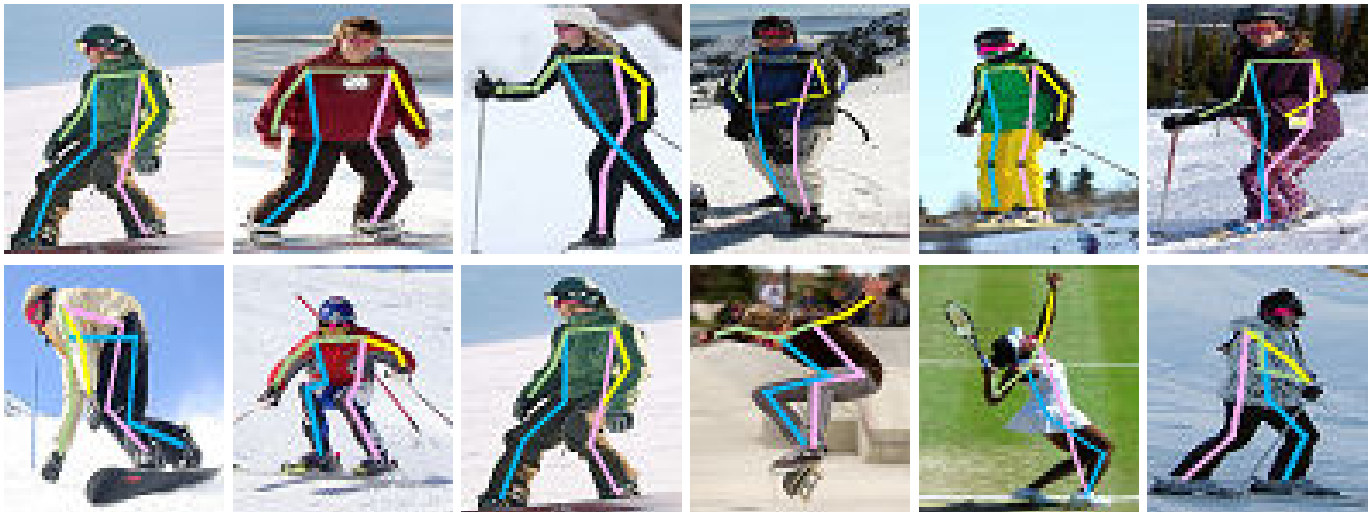


Fig. 5. Visual results of our CDKD framework on the COCO val dataset. We adopt Simcc [10] as the base model. The resolution of all images is 64×64 .

TABLE VIII
ABLATION STUDIES OF THE HYPERPARAMETERS IN THE ETHT STRATEGY ON THE MPII VALIDATION DATASET. THE τ , α , AND β REFER TO KEY HYPERPARAMETERS IN THE CDKD FRAMEWORK.

Method	Hyperparameters	PCKh@0.5 \uparrow
Non-ETHT	-	78.772
ETHT	τ	79.362
ETHT	τ, α	79.053
ETHT	τ, α, β	79.206

improve the model’s performance. It indicates our approach significantly outperforms traditional alignment methods.

Projector number. We evaluate the impact of projector number on the performance of CDKD in Table VI. The use of a projector ensemble improves the model’s performance, but an excessive number of projectors would result in a decline in performance. As shown in Table VI, the CDKD reaches the best performance when the number of projectors in SAU is 3.

Conv number. We compare the impact of the convolution number of different kernel sizes in our proposed SAU module, as shown in Table VII. we can observe that increasing moderately the proportion of convolutions with a large receptive field can further improve the performance of our proposed CDKD distillation framework. It fully demonstrates that our designed module adequately captures multi-scale human body information.

Hyperparameters. Table VIII shows how the performance of our proposed framework is affected by the choice of hyperparameters in Eq. 7 and Eq. 8. It indicates that the ETHT strategy we designed is effective. Each choice of hyperparameters helps to improve the model performance. When selecting τ as a learning object, our method reaches the best result.

TABLE IX
EVALUATION OF THE CCA MODULE IN OUR PROPOSED CDKD FRAMEWORK APPLIED UNDER DIFFERENT CONDITIONS ON THE COCO VAL DATASET.

Methods	Resolution	Role	Backbone	AP \uparrow	AR \uparrow
Simcc [10]	256×256	teacher	HRNet-48	76.4	79.4
Simcc (baseline) [10]	64×64	-	ResNet-50	40.0	45.5
CCA	64×64	student	ResNet-50	42.0 $+2.0$	47.6 $+2.1$

TABLE X
EVALUATION OF THE SAPE MODULE IN OUR PROPOSED CDKD FRAMEWORK APPLIED IN DIFFERENT MODELS ON MPII VAL DATASET. FOR CAL, THE TEACHER MODEL IS TRAINED USING THE CAL METHOD WITH A RESOLUTION OF 256×256 . FOR HRNET, THE TEACHER MODEL IS TRAINED USING THE HRNET METHOD WITH A RESOLUTION OF 256×256 .

Methods	Backbone	Resolution	PCKh@0.5 \uparrow
CAL [6]	HRNet	32×32	55.353
CAL (+SAPE)	-	32×32	56.029 $+0.676$
HRNet [3]	-	64×64	74.843
HRNet (+SAPE)	-	64×64	76.248 $+1.405$

D. Universality

We further extend our proposed CDKD framework to other pose estimation models to illustrate its universality. In current research on human pose estimation, the scope of the CCA module and the SAPE module differs significantly. Compared to the CCA module, SAPE is applicable to almost all models. Therefore, we conduct separate research on the CCA module and the SAPE module.

CCA module. We extend the CCA module to different models. As shown in Table IX, the teacher model and the student model employ distinct backbones and have varying numbers of classes. The teacher model adopts HRNet-48 as the backbone, while the student model adopts ResNet-50. The two models have noticeable differences. In this case, the

student model is still well-optimized by the CCA module, demonstrating the universality of our CCA module.

SAPE module. As an easy-to-use plug-in technique, SAPE can be seamlessly integrated into existing HPE works. As shown in Table X, our method brings comprehensive improvements to two SOTA methods based on two teacher-student pairs. It fully demonstrates the generality and effectiveness of our approach.

E. Visualized Results

Fig. 5 provides visualized human pose estimation results. As is shown in Fig. 5, the CDKD model achieves accurate human pose estimation when the input is low-resolution.

F. Limitation and Future Work

As a novel universal distillation framework, the proposed CDKD opens up many possible directions for future works to address the bottleneck limitations. Our SAPE module can be extended to various knowledge distillation tasks, enabling the distillation between features with different sizes. The CCA module we propose addresses the issue of inconsistent categories. It opens up a new perspective on distillation across categories. Nonetheless, our cross-domain knowledge distillation method is presently confined to distilling between conventional models. In the future, we plan to apply our method to large models, thus maximizing the utilization of their abundant knowledge.

V. CONCLUSION

In this work, we propose a novel low-resolution human pose estimation framework (CDKD), which includes a scale-adaptive projector ensemble (SAPE) module and a cross-class alignment (CCA) module to perform high-resolution to low-resolution knowledge distillation. In this way, the student model acquires richer image knowledge at both feature and logit levels, achieving a big leap in performance while maintaining efficiency. Extensive experiments conducted on the COCO and MPII datasets demonstrate the effectiveness of our method. In short, CDKD achieves SOTA performance among low-res methods with a low computational cost.

REFERENCES

- [1] T.-Y. Lin, M. Maire, S. Belongie, J. Hays, P. Perona, D. Ramanan, P. Dollár, and C. L. Zitnick, "Microsoft coco: Common objects in context," in *Computer Vision—ECCV 2014: 13th European Conference, Zurich, Switzerland, September 6–12, 2014, Proceedings, Part V 13*. Springer, 2014, pp. 740–755.
- [2] M. Andriluka, L. Pishchulin, P. Gehler, and B. Schiele, "2d human pose estimation: New benchmark and state of the art analysis," in *Proceedings of the IEEE Conference on Computer Vision and Pattern Recognition*, 2014, pp. 3686–3693.
- [3] K. Sun, B. Xiao, D. Liu, and J. Wang, "Deep high-resolution representation learning for human pose estimation," in *Proceedings of the IEEE/CVF conference on computer vision and pattern recognition*, 2019, pp. 5693–5703.
- [4] B. Xiao, H. Wu, and Y. Wei, "Simple baselines for human pose estimation and tracking," in *Proceedings of the European conference on computer vision (ECCV)*, 2018, pp. 466–481.
- [5] F. Zhang, X. Zhu, H. Dai, M. Ye, and C. Zhu, "Distribution-aware coordinate representation for human pose estimation," in *Proceedings of the IEEE/CVF conference on computer vision and pattern recognition*, 2020, pp. 7093–7102.
- [6] C. Wang, F. Zhang, X. Zhu, and S. S. Ge, "Low-resolution human pose estimation," *Pattern Recognition*, vol. 126, p. 108579, 2022.
- [7] Z. Li, J. Ye, M. Song, Y. Huang, and Z. Pan, "Online knowledge distillation for efficient pose estimation," in *Proceedings of the IEEE/CVF international conference on computer vision*, 2021, pp. 11 740–11 750.
- [8] Y. Li, S. Zhang, Z. Wang, S. Yang, W. Yang, S.-T. Xia, and E. Zhou, "Tokenpose: Learning keypoint tokens for human pose estimation," in *Proceedings of the IEEE/CVF International conference on computer vision*, 2021, pp. 11 313–11 322.
- [9] K. Li, S. Wang, X. Zhang, Y. Xu, W. Xu, and Z. Tu, "Pose recognition with cascade transformers," in *Proceedings of the IEEE/CVF conference on computer vision and pattern recognition*, 2021, pp. 1944–1953.
- [10] Y. Li, S. Yang, P. Liu, S. Zhang, Y. Wang, Z. Wang, W. Yang, and S.-T. Xia, "Simcc: A simple coordinate classification perspective for human pose estimation," in *European Conference on Computer Vision*. Springer, 2022, pp. 89–106.
- [11] J. Li, S. Bian, A. Zeng, C. Wang, B. Pang, W. Liu, and C. Lu, "Human pose regression with residual log-likelihood estimation," in *Proceedings of the IEEE/CVF international conference on computer vision*, 2021, pp. 11 025–11 034.
- [12] Z.-H. Zhou, J. Wu, and W. Tang, "Ensembling neural networks: many could be better than all," *Artificial intelligence*, vol. 137, no. 1-2, pp. 239–263, 2002.
- [13] L. Qi, J. Kuen, J. Gu, Z. Lin, Y. Wang, Y. Chen, Y. Li, and J. Jia, "Multi-scale aligned distillation for low-resolution detection," in *Proceedings of the IEEE/CVF Conference on Computer Vision and Pattern Recognition*, 2021, pp. 14 443–14 453.
- [14] Z. Huang, S. Yang, M. Zhou, Z. Li, Z. Gong, and Y. Chen, "Feature map distillation of thin nets for low-resolution object recognition," *IEEE Transactions on Image Processing*, vol. 31, pp. 1364–1379, 2022.
- [15] S. Shin, J. Lee, J. Lee, Y. Yu, and K. Lee, "Teaching where to look: Attention similarity knowledge distillation for low resolution face recognition," in *European Conference on Computer Vision*. Springer, 2022, pp. 631–647.
- [16] Y. Jin, J. Wang, and D. Lin, "Multi-level logit distillation," in *Proceedings of the IEEE/CVF Conference on Computer Vision and Pattern Recognition*, 2023, pp. 24 276–24 285.
- [17] X. Deng and Z. Zhang, "Comprehensive knowledge distillation with causal intervention," *Advances in Neural Information Processing Systems*, vol. 34, pp. 22 158–22 170, 2021.
- [18] Y. Chen, S. Wang, J. Liu, X. Xu, F. de Hoog, and Z. Huang, "Improved feature distillation via projector ensemble," *Advances in Neural Information Processing Systems*, vol. 35, pp. 12 084–12 095, 2022.
- [19] R. Diaz and A. Marathe, "Soft labels for ordinal regression," in *Proceedings of the IEEE/CVF conference on computer vision and pattern recognition*, 2019, pp. 4738–4747.
- [20] X. Li, W. Wang, X. Hu, and J. Yang, "Selective kernel networks," in *Proceedings of the IEEE/CVF conference on computer vision and pattern recognition*, 2019, pp. 510–519.
- [21] Z. Li, X. Li, L. Yang, B. Zhao, R. Song, L. Luo, J. Li, and J. Yang, "Curriculum temperature for knowledge distillation," in *Proceedings of the AAAI Conference on Artificial Intelligence*, vol. 37, no. 2, 2023, pp. 1504–1512.
- [22] F. Zhang, X. Zhu, and M. Ye, "Fast human pose estimation," in *Proceedings of the IEEE/CVF conference on computer vision and pattern recognition*, 2019, pp. 3517–3526.
- [23] Z. Geng, C. Wang, Y. Wei, Z. Liu, H. Li, and H. Hu, "Human pose as compositional tokens," in *Proceedings of the IEEE/CVF Conference on Computer Vision and Pattern Recognition*, 2023, pp. 660–671.
- [24] Y. Zhu, Q. Zhou, N. Liu, Z. Xu, Z. Ou, X. Mou, and J. Tang, "Scalekd: Distilling scale-aware knowledge in small object detector," in *Proceedings of the IEEE/CVF Conference on Computer Vision and Pattern Recognition*, 2023, pp. 19 723–19 733.
- [25] Z. Yang, A. Zeng, C. Yuan, and Y. Li, "Effective whole-body pose estimation with two-stages distillation," in *Proceedings of the IEEE/CVF International Conference on Computer Vision*, 2023, pp. 4210–4220.
- [26] W. Huang, Z. Peng, L. Dong, F. Wei, J. Jiao, and Q. Ye, "Generic-to-specific distillation of masked autoencoders," in *Proceedings of the IEEE/CVF Conference on Computer Vision and Pattern Recognition*, 2023, pp. 15 996–16 005.
- [27] B. Zhao, Q. Cui, R. Song, Y. Qiu, and J. Liang, "Decoupled knowledge distillation," in *Proceedings of the IEEE/CVF Conference on computer vision and pattern recognition*, 2022, pp. 11 953–11 962.
- [28] A. Vats and D. C. Anastasiu, "Key point-based driver activity recognition," in *Proceedings of the IEEE/CVF Conference on Computer Vision and Pattern Recognition*, 2022, pp. 3274–3281.

- [29] U. Iqbal, P. Molchanov, and J. Kautz, “Weakly-supervised 3d human pose learning via multi-view images in the wild,” in *Proceedings of the IEEE/CVF conference on computer vision and pattern recognition*, 2020, pp. 5243–5252.
- [30] Y. Cheng, B. Wang, and R. T. Tan, “Dual networks based 3d multi-person pose estimation from monocular video,” *IEEE Transactions on Pattern Analysis and Machine Intelligence*, vol. 45, no. 2, pp. 1636–1651, 2022.
- [31] S. Ye, Y. Zhang, J. Hu, L. Cao, S. Zhang, L. Shen, J. Wang, S. Ding, and R. Ji, “Distilpose: Tokenized pose regression with heatmap distillation,” in *Proceedings of the IEEE/CVF Conference on Computer Vision and Pattern Recognition*, 2023, pp. 2163–2172.
- [32] J. Wang, K. Sun, T. Cheng, B. Jiang, C. Deng, Y. Zhao, D. Liu, Y. Mu, M. Tan, X. Wang *et al.*, “Deep high-resolution representation learning for visual recognition,” *IEEE transactions on pattern analysis and machine intelligence*, vol. 43, no. 10, pp. 3349–3364, 2020.
- [33] L. Schmidtke, A. Vlontzos, S. Ellershaw, A. Lukens, T. Arichi, and B. Kainz, “Unsupervised human pose estimation through transforming shape templates,” in *Proceedings of the IEEE/CVF Conference on Computer Vision and Pattern Recognition*, 2021, pp. 2484–2494.
- [34] J. Kim, H. Lee, and S. S. Woo, “Imf: integrating matched features using attentive logit in knowledge distillation,” in *Proceedings of the Thirty-Second International Joint Conference on Artificial Intelligence IJCAI*, 2023.
- [35] Z. Ni, F. Yang, S. Wen, and G. Zhang, “Dual relation knowledge distillation for object detection,” *arXiv preprint arXiv:2302.05637*, 2023.
- [36] A. Romero, N. Ballas, S. E. Kahou, A. Chassang, C. Gatta, and Y. Bengio, “Fitnets: Hints for thin deep nets,” *arXiv preprint arXiv:1412.6550*, 2014.
- [37] S. Ge, S. Zhao, C. Li, Y. Zhang, and J. Li, “Efficient low-resolution face recognition via bridge distillation,” *IEEE Transactions on Image Processing*, vol. 29, pp. 6898–6908, 2020.
- [38] A. Kumar and R. Chellappa, “S2ld: Semi-supervised landmark detection in low-resolution images and impact on face verification,” in *Proceedings of the IEEE/CVF conference on computer vision and pattern recognition workshops*, 2020, pp. 758–759.
- [39] J. C. L. Chai, T.-S. Ng, C.-Y. Low, J. Park, and A. B. J. Teoh, “Recognizability embedding enhancement for very low-resolution face recognition and quality estimation,” in *Proceedings of the IEEE/CVF Conference on Computer Vision and Pattern Recognition*, 2023, pp. 9957–9967.
- [40] R. Sunkara and T. Luo, “No more strided convolutions or pooling: A new cnn building block for low-resolution images and small objects,” in *Joint European Conference on Machine Learning and Knowledge Discovery in Databases*. Springer, 2022, pp. 443–459.
- [41] X. Xu, H. Chen, F. Moreno-Noguer, L. A. Jeni, and F. De la Torre, “3d human shape and pose from a single low-resolution image with self-supervised learning,” in *Computer Vision—ECCV 2020: 16th European Conference, Glasgow, UK, August 23–28, 2020, Proceedings, Part IX 16*. Springer, 2020, pp. 284–300.
- [42] R. Miles, I. Elezi, and J. Deng, “*v_kd*: improving knowledge distillation using orthogonal projections,” *arXiv preprint arXiv:2403.06213*, 2024.
- [43] J. Wang, Y. Chen, Z. Zheng, X. Li, M.-M. Cheng, and Q. Hou, “Crosskd: Cross-head knowledge distillation for object detection.”
- [44] Z. Zheng, R. Ye, P. Wang, D. Ren, W. Zuo, Q. Hou, and M.-M. Cheng, “Localization distillation for dense object detection,” in *Proceedings of the IEEE/CVF Conference on Computer Vision and Pattern Recognition*, 2022, pp. 9407–9416.
- [45] B. Artacho and A. Savakis, “Unipose: Unified human pose estimation in single images and videos,” in *Proceedings of the IEEE/CVF conference on computer vision and pattern recognition*, 2020, pp. 7035–7044.
- [46] S.-E. Wei, V. Ramakrishna, T. Kanade, and Y. Sheikh, “Convolutional pose machines,” in *Proceedings of the IEEE conference on Computer Vision and Pattern Recognition*, 2016, pp. 4724–4732.
- [47] Y. Chen, Z. Wang, Y. Peng, Z. Zhang, G. Yu, and J. Sun, “Cascaded pyramid network for multi-person pose estimation,” in *Proceedings of the IEEE conference on computer vision and pattern recognition*, 2018, pp. 7103–7112.
- [48] A. Newell, K. Yang, and J. Deng, “Stacked hourglass networks for human pose estimation,” in *Computer Vision—ECCV 2016: 14th European Conference, Amsterdam, The Netherlands, October 11–14, 2016, Proceedings, Part VIII 14*. Springer, 2016, pp. 483–499.
- [49] J. Huang, Z. Zhu, F. Guo, and G. Huang, “The devil is in the details: Delving into unbiased data processing for human pose estimation,” in *Proceedings of the IEEE/CVF conference on computer vision and pattern recognition*, 2020, pp. 5700–5709.
- [50] Z. Cao, T. Simon, S.-E. Wei, and Y. Sheikh, “Realtime multi-person 2d pose estimation using part affinity fields,” in *Proceedings of the IEEE conference on computer vision and pattern recognition*, 2017, pp. 7291–7299.
- [51] H.-S. Fang, S. Xie, Y.-W. Tai, and C. Lu, “Rmpe: Regional multi-person pose estimation,” in *Proceedings of the IEEE international conference on computer vision*, 2017, pp. 2334–2343.
- [52] W. Li, Z. Wang, B. Yin, Q. Peng, Y. Du, T. Xiao, G. Yu, H. Lu, Y. Wei, and J. Sun, “Rethinking on multi-stage networks for human pose estimation,” *arXiv preprint arXiv:1901.00148*, 2019.
- [53] Y. Wang, M. Li, H. Cai, W.-M. Chen, and S. Han, “Lite pose: Efficient architecture design for 2d human pose estimation,” in *Proceedings of the IEEE/CVF Conference on Computer Vision and Pattern Recognition*, 2022, pp. 13 126–13 136.
- [54] Z. Geng, K. Sun, B. Xiao, Z. Zhang, and J. Wang, “Bottom-up human pose estimation via disentangled keypoint regression,” in *Proceedings of the IEEE/CVF conference on computer vision and pattern recognition*, 2021, pp. 14 676–14 686.
- [55] F. Wei, X. Sun, H. Li, J. Wang, and S. Lin, “Point-set anchors for object detection, instance segmentation and pose estimation,” in *Computer Vision—ECCV 2020: 16th European Conference, Glasgow, UK, August 23–28, 2020, Proceedings, Part X 16*. Springer, 2020, pp. 527–544.
- [56] V. Belagiannis, C. Rupprecht, G. Carneiro, and N. Navab, “Robust optimization for deep regression,” in *Proceedings of the IEEE international conference on computer vision*, 2015, pp. 2830–2838.
- [57] J. Carreira, P. Agrawal, K. Fragkiadaki, and J. Malik, “Human pose estimation with iterative error feedback,” in *Proceedings of the IEEE conference on computer vision and pattern recognition*, 2016, pp. 4733–4742.
- [58] Z. Tian, H. Chen, and C. Shen, “Directpose: Direct end-to-end multi-person pose estimation,” *arXiv preprint arXiv:1911.07451*, 2019.
- [59] A. Toshev and C. Szegedy, “DeepPose: Human pose estimation via deep neural networks,” in *Proceedings of the IEEE conference on computer vision and pattern recognition*, 2014, pp. 1653–1660.
- [60] X. Zhou, D. Wang, and P. Krähenbühl, “Objects as points,” *arXiv preprint arXiv:1904.07850*, 2019.
- [61] M. Sandler, A. Zhmoginov, A. G. Howard, and P. K. Mudrakarta, “Parameter-efficient multi-task and transfer learning,” Jun. 13 2023, uS Patent 11,676,008.
- [62] S. Ge, S. Zhao, C. Li, and J. Li, “Low-resolution face recognition in the wild via selective knowledge distillation,” *IEEE Transactions on Image Processing*, vol. 28, no. 4, pp. 2051–2062, 2018.
- [63] T. Vu, C. Van Nguyen, T. X. Pham, T. M. Luu, and C. D. Yoo, “Fast and efficient image quality enhancement via desubpixel convolutional neural networks,” in *Proceedings of the European Conference on Computer Vision (ECCV) Workshops*, 2018, pp. 0–0.
- [64] Q. Wang, B. Wu, P. Zhu, P. Li, W. Zuo, and Q. Hu, “Eca-net: Efficient channel attention for deep convolutional neural networks,” in *Proceedings of the IEEE/CVF conference on computer vision and pattern recognition*, 2020, pp. 11 534–11 542.
- [65] G. Papandreou, T. Zhu, N. Kanazawa, A. Toshev, J. Tompson, C. Brengle, and K. Murphy, “Towards accurate multi-person pose estimation in the wild,” in *Proceedings of the IEEE conference on computer vision and pattern recognition*, 2017, pp. 4903–4911.
- [66] D.-M. Pham, “Human identification using neural network-based classification of periodic behaviors in virtual reality,” in *2018 IEEE Conference on Virtual Reality and 3D User Interfaces (VR)*. IEEE, 2018, pp. 657–658.
- [67] I. S. MacKenzie, “Human-computer interaction: An empirical research perspective,” 2012.
- [68] H. Qu, L. Xu, Y. Cai, L. G. Foo, and J. Liu, “Heatmap distribution matching for human pose estimation,” *Advances in Neural Information Processing Systems*, vol. 35, pp. 24 327–24 339, 2022.
- [69] Y. Xu, J. Zhang, Q. Zhang, and D. Tao, “Vitpose: Simple vision transformer baselines for human pose estimation,” *Advances in Neural Information Processing Systems*, vol. 35, pp. 38 571–38 584, 2022.
- [70] S. Yang, Z. Quan, M. Nie, and W. Yang, “Transpose: Keypoint localization via transformer,” in *Proceedings of the IEEE/CVF International Conference on Computer Vision*, 2021, pp. 11 802–11 812.
- [71] J. Kuen, X. Kong, Z. Lin, G. Wang, J. Yin, S. See, and Y.-P. Tan, “Stochastic downsampling for cost-adjustable inference and improved regularization in convolutional networks,” in *Proceedings of the IEEE Conference on Computer Vision and Pattern Recognition*, 2018, pp. 7929–7938.

- [72] D. Li, A. Yao, and Q. Chen, "Learning to learn parameterized classification networks for scalable input images," in *Computer Vision—ECCV 2020: 16th European Conference, Glasgow, UK, August 23–28, 2020, Proceedings, Part XXIX 16*. Springer, 2020, pp. 19–35.
- [73] D. Morrison, A. W. Tow, M. McTaggart, R. Smith, N. Kelly-Boxall, S. Wade-McCue, J. Erskine, R. Grinover, A. Gurman, T. Hunn *et al.*, "Cartman: The low-cost cartesian manipulator that won the amazon robotics challenge," in *2018 IEEE International Conference on Robotics and Automation (ICRA)*. IEEE, 2018, pp. 7757–7764.
- [74] Y. Wang, F. Sun, D. Li, and A. Yao, "Resolution switchable networks for runtime efficient image recognition," in *Computer Vision—ECCV 2020: 16th European Conference, Glasgow, UK, August 23–28, 2020, Proceedings, Part XV 16*. Springer, 2020, pp. 533–549.
- [75] A. Bulat and G. Tzimiropoulos, "Human pose estimation via convolutional part heatmap regression," in *Computer Vision—ECCV 2016: 14th European Conference, Amsterdam, The Netherlands, October 11–14, 2016, Proceedings, Part VII 14*. Springer, 2016, pp. 717–732.
- [76] J. J. Tompson, A. Jain, Y. LeCun, and C. Bregler, "Joint training of a convolutional network and a graphical model for human pose estimation," *Advances in neural information processing systems*, vol. 27, 2014.
- [77] A. Varamesh and T. Tuytelaars, "Mixture dense regression for object detection and human pose estimation," in *Proceedings of the IEEE/CVF conference on computer vision and pattern recognition*, 2020, pp. 13 086–13 095.
- [78] A. Vaswani, N. Shazeer, N. Parmar, J. Uszkoreit, L. Jones, A. N. Gomez, Ł. Kaiser, and I. Polosukhin, "Attention is all you need," *Advances in neural information processing systems*, vol. 30, 2017.
- [79] Z. Kan, S. Chen, C. Zhang, Y. Tang, and Z. He, "Self-correctable and adaptable inference for generalizable human pose estimation," in *Proceedings of the IEEE/CVF Conference on Computer Vision and Pattern Recognition*, 2023, pp. 5537–5546.
- [80] X. Peng, J. Hoffman, X. Y. Stella, and K. Saenko, "Fine-to-coarse knowledge transfer for low-res image classification," in *2016 IEEE International Conference on Image Processing (ICIP)*. IEEE, 2016, pp. 3683–3687.
- [81] M. Singh, S. Nagpal, M. Vatsa, and R. Singh, "Enhancing fine-grained classification for low resolution images," in *2021 International Joint Conference on Neural Networks (IJCNN)*. IEEE, 2021, pp. 1–8.
- [82] Z. Zou and W. Tang, "Modulated graph convolutional network for 3d human pose estimation," in *Proceedings of the IEEE/CVF international conference on computer vision*, 2021, pp. 11 477–11 487.
- [83] J. Redmon, S. Divvala, R. Girshick, and A. Farhadi, "You only look once: Unified, real-time object detection," in *Proceedings of the IEEE conference on computer vision and pattern recognition*, 2016, pp. 779–788.
- [84] K. He, X. Zhang, S. Ren, and J. Sun, "Deep residual learning for image recognition," in *Proceedings of the IEEE conference on computer vision and pattern recognition*, 2016, pp. 770–778.
- [85] A. Krizhevsky, V. Nair, and G. Hinton, "Cifar-10 (canadian institute for advanced research)," URL <http://www.cs.toronto.edu/kriz/cifar.html>, vol. 5, no. 4, p. 1, 2010.
- [86] Y. Le and X. Yang, "Tiny imagenet visual recognition challenge," *CS 231N*, vol. 7, no. 7, p. 3, 2015.
- [87] L. Zhao, X. Peng, Y. Tian, M. Kapadia, and D. N. Metaxas, "Semantic graph convolutional networks for 3d human pose regression," in *Proceedings of the IEEE/CVF conference on computer vision and pattern recognition*, 2019, pp. 3425–3435.
- [88] S.-H. Zhang, R. Li, X. Dong, P. Rosin, Z. Cai, X. Han, D. Yang, H. Huang, and S.-M. Hu, "Pose2seg: Detection free human instance segmentation," in *Proceedings of the IEEE/CVF conference on computer vision and pattern recognition*, 2019, pp. 889–898.
- [89] A. Zeng, X. Sun, F. Huang, M. Liu, Q. Xu, and S. Lin, "Smet: Improving generalization in 3d human pose estimation with a split-and-recombine approach," in *Computer Vision—ECCV 2020: 16th European Conference, Glasgow, UK, August 23–28, 2020, Proceedings, Part XIV 16*. Springer, 2020, pp. 507–523.
- [90] W. Yang, W. Ouyang, H. Li, and X. Wang, "End-to-end learning of deformable mixture of parts and deep convolutional neural networks for human pose estimation," in *Proceedings of the IEEE conference on computer vision and pattern recognition*, 2016, pp. 3073–3082.
- [91] W. Yang, S. Li, W. Ouyang, H. Li, and X. Wang, "Learning feature pyramids for human pose estimation," in *proceedings of the IEEE international conference on computer vision*, 2017, pp. 1281–1290.
- [92] T. Xu and W. Takano, "Graph stacked hourglass networks for 3d human pose estimation," in *Proceedings of the IEEE/CVF conference on computer vision and pattern recognition*, 2021, pp. 16 105–16 114.
- [93] K. Sun, C. Lan, J. Xing, W. Zeng, D. Liu, and J. Wang, "Human pose estimation using global and local normalization," in *Proceedings of the IEEE international conference on computer vision*, 2017, pp. 5599–5607.
- [94] K. Su, D. Yu, Z. Xu, X. Geng, and C. Wang, "Multi-person pose estimation with enhanced channel-wise and spatial information," in *Proceedings of the IEEE/CVF conference on computer vision and pattern recognition*, 2019, pp. 5674–5682.
- [95] D. Shi, X. Wei, L. Li, Y. Ren, and W. Tan, "End-to-end multi-person pose estimation with transformers," in *Proceedings of the IEEE/CVF Conference on Computer Vision and Pattern Recognition*, 2022, pp. 11 069–11 078.
- [96] S. Sharma, P. T. Varigonda, P. Bindal, A. Sharma, and A. Jain, "Monocular 3d human pose estimation by generation and ordinal ranking," in *Proceedings of the IEEE/CVF international conference on computer vision*, 2019, pp. 2325–2334.
- [97] S. Lee, J. Rim, B. Jeong, G. Kim, B. Woo, H. Lee, S. Cho, and S. Kwak, "Human pose estimation in extremely low-light conditions," in *Proceedings of the IEEE/CVF Conference on Computer Vision and Pattern Recognition*, 2023, pp. 704–714.
- [98] X. Ju, A. Zeng, J. Wang, Q. Xu, and L. Zhang, "Human-art: A versatile human-centric dataset bridging natural and artificial scenes," in *Proceedings of the IEEE/CVF Conference on Computer Vision and Pattern Recognition*, 2023, pp. 618–629.
- [99] J. Yang, A. Zeng, S. Liu, F. Li, R. Zhang, and L. Zhang, "Explicit box detection unifies end-to-end multi-person pose estimation," *arXiv preprint arXiv:2302.01593*, 2023.
- [100] G. Jocher, A. Chaurasia, A. Stoken, J. Borovec, Y. Kwon, K. Michael, J. Fang, Z. Yifu, C. Wong, D. Montes *et al.*, "ultralytics/yolov5: v7.0-yolov5 sota realtime instance segmentation," *Zenodo*, 2022.
- [101] P. Jeevan and A. Sethi, "Wavemix: resource-efficient token mixing for images," *arXiv preprint arXiv:2203.03689*, 2022.
- [102] G. Huang, Y. Sun, Z. Liu, D. Sedra, and K. Q. Weinberger, "Deep networks with stochastic depth," in *Computer Vision—ECCV 2016: 14th European Conference, Amsterdam, The Netherlands, October 11–14, 2016, Proceedings, Part IV 14*. Springer, 2016, pp. 646–661.
- [103] G. G. Chrysos, S. Moschoglou, G. Bouritsas, J. Deng, Y. Panagakis, and S. Zafeiriou, "Deep polynomial neural networks," *IEEE transactions on pattern analysis and machine intelligence*, vol. 44, no. 8, pp. 4021–4034, 2021.
- [104] Y. Xiong, Z. Zeng, R. Chakraborty, M. Tan, G. Fung, Y. Li, and V. Singh, "Nyströmformer: A nyström-based algorithm for approximating self-attention," in *Proceedings of the AAAI Conference on Artificial Intelligence*, vol. 35, no. 16, 2021, pp. 14 138–14 148.
- [105] B. Koonce and B. Koonce, "Resnet 50," *Convolutional neural networks with swift for tensorflow: image recognition and dataset categorization*, pp. 63–72, 2021.
- [106] S. Targ, D. Almeida, and K. Lyman, "Resnet in resnet: Generalizing residual architectures," *arXiv preprint arXiv:1603.08029*, 2016.
- [107] X. Nie, J. Feng, J. Zhang, and S. Yan, "Single-stage multi-person pose machines," in *Proceedings of the IEEE/CVF international conference on computer vision*, 2019, pp. 6951–6960.
- [108] Q. Sun, Y. Wang, A. Zeng, W. Yin, C. Wei, W. Wang, H. Mei, C. S. Leung, Z. Liu, L. Yang *et al.*, "Aios: All-in-one-stage expressive human pose and shape estimation," *arXiv preprint arXiv:2403.17934*, 2024.
- [109] G. Hinton, O. Vinyals, and J. Dean, "Distilling the knowledge in a neural network," *arXiv preprint arXiv:1503.02531*, 2015.
- [110] B. Heo, J. Kim, S. Yun, H. Park, N. Kwak, and J. Y. Choi, "A comprehensive overhaul of feature distillation," in *Proceedings of the IEEE/CVF International Conference on Computer Vision*, 2019, pp. 1921–1930.
- [111] B. Heo, M. Lee, S. Yun, and J. Y. Choi, "Knowledge transfer via distillation of activation boundaries formed by hidden neurons," in *Proceedings of the AAAI conference on artificial intelligence*, vol. 33, no. 01, 2019, pp. 3779–3787.
- [112] W. Park, D. Kim, Y. Lu, and M. Cho, "Relational knowledge distillation," in *Proceedings of the IEEE/CVF conference on computer vision and pattern recognition*, 2019, pp. 3967–3976.
- [113] Y. Tian, D. Krishnan, and P. Isola, "Contrastive representation distillation," *arXiv preprint arXiv:1910.10699*, 2019.
- [114] T.-Y. Lin, P. Dollár, R. Girshick, K. He, B. Hariharan, and S. Belongie, "Feature pyramid networks for object detection," in *Proceedings of the IEEE conference on computer vision and pattern recognition*, 2017, pp. 2117–2125.
- [115] J. Guo, M. Chen, Y. Hu, C. Zhu, X. He, and D. Cai, "Reducing the teacher-student gap via spherical knowledge distillation," *arXiv preprint arXiv:2010.07485*, 2020.

- [116] Y. Niu, L. Chen, C. Zhou, and H. Zhang, “Respecting transfer gap in knowledge distillation,” *Advances in Neural Information Processing Systems*, vol. 35, pp. 21 933–21 947, 2022.
- [117] H. Liu, T. Liu, Y. Chen, Z. Zhang, and Y.-F. Li, “Ehpe: Skeleton cues-based gaussian coordinate encoding for efficient human pose estimation,” *IEEE Transactions on Multimedia*, 2022.
- [118] W. Li, H. Liu, R. Ding, M. Liu, P. Wang, and W. Yang, “Exploiting temporal contexts with strided transformer for 3d human pose estimation,” *IEEE Transactions on Multimedia*, vol. 25, pp. 1282–1293, 2022.
- [119] M. Li, Z. Zhou, and X. Liu, “Multi-person pose estimation using bounding box constraint and lstm,” *IEEE Transactions on Multimedia*, vol. 21, no. 10, pp. 2653–2663, 2019.
- [120] S. Zou, X. Zuo, S. Wang, Y. Qian, C. Guo, and L. Cheng, “Human pose and shape estimation from single polarization images,” *IEEE Transactions on Multimedia*, 2022.
- [121] G. Ning, Z. Zhang, and Z. He, “Knowledge-guided deep fractal neural networks for human pose estimation,” *IEEE Transactions on Multimedia*, vol. 20, no. 5, pp. 1246–1259, 2017.